TU Delft

Delft University of Technology

Dynamic Inversion Heat-Flux Tracking for Hypersonic Entry

Mooij, E.

DOI
10.2514/6.2023-2499

Publication date
2023

Document Version
Final published version

Published in
AIAA SciTech Forum 2023

Citation (APA)
Mooij, E. (2023). Dynamic Inversion Heat-Flux Tracking for Hypersonic Entry. In *AIAA SciTech Forum 2023* Article AIAA 2023-2499 https://doi.org/10.2514/6.2023-2499

Important note
To cite this publication, please use the final published version (if applicable).
Please check the document version above.

Copyright
Other than for strictly personal use, it is not permitted to download, forward or distribute the text or part of it, without the consent of the author(s) and/or copyright holder(s), unless the work is under an open content license such as Creative Commons.

Takedown policy
Please contact us and provide details if you believe this document breaches copyrights.
We will remove access to the work immediately and investigate your claim.

This work is downloaded from Delft University of Technology.
For technical reasons the number of authors shown on this cover page is limited to a maximum of 10.

Dynamic Inversion Heat-Flux Tracking for Hypersonic Entry

Erwin Mooij*

Delft University of Technology, Faculty of Aerospace Engineering,

Kluyverweg 1, 2629 HS Delft, The Netherlands

To limit the mass of the vehicle's thermal protection system, an optimal trajectory that minimises the total integrated heat load should be flown. This means that the maximum heat-flux constraint is followed for as long as possible, until the maximum mechanical load is encountered. Flying as close to this load as possible contributes to minimising the heat load as well. The guidance system to track the path constraints includes two components: a semi-analytical guidance that produces nominal bank-angle commands and a tracking system based on non-linear dynamic inversion. The flight system under consideration is a hypersonic test vehicle of which the stagnation heat-flux should not exceed 1,700 kW/m^2, with a limit of the mechanical load of 4.8 g. The preliminary results show that the tracking system extends the duration of heat-flux tracking and is able to tightly track the heat-flux constraint, but reduces the flight range because of that. A simultaneous optimisation of these two conflicting objectives should be pursued to refine the guidance-system design in case both have requirements to be met. In none of the cases considered, the *g-load* constraint was violated, although a more detailed analysis is required to make this part of the guidance more robust.

I. Introduction

With the continuing effort to develop robust and reusable thermal protection systems (TPSs) for re-entry vehicles, the use of experimental test vehicles is a crucial element in the design methodology. Laboratory conditions are not representative for the hypersonic flight conditions, and also hypersonic windtunnels and plasmatunnels cannot combine the hyper-velociy thermal conditions with pressure and Reynolds number. Scaleability effects of the (small) wind-tunnel models to realistic vehicle sizes, as well as the (very) short measurement times, are other aspects that severely limit the study of the hypersonic flow environment.

A small and low-cost re-entry vehicle can be a good means for testing new heat-resistant materials and qualifying newly developed sub-systems in a realistic flight environment, to complement ground tests and numerical experiments. The disadvantage of using ballistic vehicles is not just the relatively short flight time, but the extreme thermo-mechanical loads that are beyond the capabilities of reusable TPS. This can be overcome by actively controlling the aerodynamic forces acting on the re-entry vehicle, like the COLIBRI (COncepts of LIfting Bodies for Re-entry Investigations).[1] More recent examples are the German SHarp Edge Flight EXperiment (SHEFEX) vehicles that aimed to investigate possible new shapes for future launchers or re-entry vehicles.[2–5] SHEFEX-1 and -2 were launched in 2006 and 2012, respectively.

A vehicle that could potentially fulfil similar mission requirements is *Hyperion-1*, a small re-entry testbed originally conceived in the mid nineties,[6] see Fig. 1. In subsequent studies, the focus was on one of the requirements, namely to test new, heat-resistant materials under realistic re-entry conditions. For that reason, a flight along the maximum heat-flux constraint was defined, which would maximise the measurement time along this constraint, but at the same time yield a minimum integrated heat load and thus a minimal TPS mass. To achieve such a flight, a constraint-tracking guidance was developed and tested, using a combination of an analytical nominal guidance and a tracking algorithm.[7–9] As tracking guidance, both a

*Associate Professor, Section Astrodynamics and Space Missions, e.mooij@tudelft.nl, Associate Fellow AIAA.

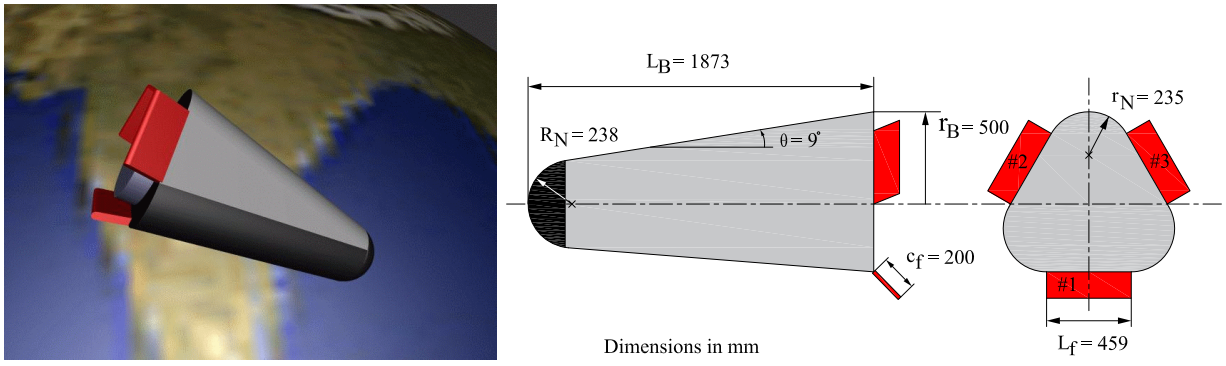

(a) Artist impression (b) Geometry

Figure 1. *Hyperion-1* **re-entry vehicle.**

linear quadratic regulator with output weighting and a concept based on simple adaptive control was used, as well as the combination of the two. Ref. 9 concluded that the combination of an inner-loop and outer-loop guidance performed the best, but that potentially the robustness has to be improved when more vehicle uncertainties and environmental perturbations are included.

To eliminate non-linearities in the system by cancelling them out with state feedback, Non-linear Dynamic Inversion (NDI) controllers were developed. This kind of robust control, however, can only work when an accurate on-board dynamics model is available. To alleviate this dependency, several modifications to the NDI framework have been proposed, one of them being the concept of Incremental Non-linear Dynamic Inversion (INDI). This concept has been very successful as attitude controller: by making use of actuator output and angular-acceleration measurement feedback the desired closed-loop dynamics does not come from explicit model following, but are the implicit result from closing the feedback loops.[10,11]

In the current study, the concept of INDI cannot be applied to the tracking component of the guidance system, though, because this tracking (of the heat flux) is centred around a (linearised) error-dynamics model. In that case the concept of INDI reduces to (Non-)Linear Dynamics Inversion (NDI).

The paper is subsequently organised as follows. In Sec. II the dynamics model of the re-entry vehicle is discussed. Since the guidance system is focussed on controlling the heat flux, without considering the induced lateral motion, only the planar motion, *i.e.,* the motion in the vertical plane, is considered. From the given non-linear equations of motion, a state-space model is derived that links the velocity and so-called pseudo altitude to the heat-flux error dynamics model. Section III.B will summarise the theoretical background of INDI and NDI, and formulate the tracking-guidance system. In Sec. IV, first the results of the nominal re-entry mission is presented, after which the robustness of the guidance system is addressed. Section V, finally, concludes this paper with some final remarks.

II. Re-entry Planar Motion

A. Flight Dynamics

For a spherical Earth with a central gravity field, the equations of motion used as starting point for the guidance-system design are given by:

$$\dot{V} = \omega_{cb}^2 R \sin\gamma - g\sin\gamma - \frac{D}{m} \tag{1}$$

$$V\dot{\gamma} = 2\omega_{cb}V + \frac{V^2}{R}\cos\gamma + \omega_{cb}^2 R\cos\gamma - g\cos\gamma + \frac{L}{m}\cos\sigma \tag{2}$$

$$\dot{h} = V\sin\gamma \tag{3}$$

The controls for translational motion are the angle of attack and bank angle, commands that are output from the guidance system. The angle of attack drives the magnitude of the aerodynamic drag and lift, whereas the bank angle defines the lift orientation. It is duly noted that the out-of-plane motion induced by banking the vehicle is currently ignored; banking would change the heading away from the equator and change

the latitude. The induced offset from the nominal ground track is typically dealt with a separate component of the guidance system, the so-called lateral guidance. Development of such system and integrating it with the constraint tracking is left as future work.

Because the altitude is a kinematic variable it cannot be directly controlled, only indirectly by changing the flight-path angle. Therefore, for the sake of the tracking-guidance design, h and γ are combined into a so-called pseudo altitude, h^*:

$$h^* = h + K_\gamma \gamma \tag{4}$$

where K_γ is a velocity-dependent gain, *i.e.,* $K_\gamma = c_\gamma V$ m/rad; a value of $c_\gamma = 20$ s/rad is found to work well for this type of vehicle-mission combination.[7]

From Eq. (4) we find

$$\dot{h}^* = \dot{h} + \dot{K}_\gamma \gamma + K_\gamma \dot{\gamma} = \dot{h} + c_\gamma \dot{V} \gamma + c_\gamma V \dot{\gamma} \tag{5}$$

such that, with Eqs. (2) and (3), $\dot{h}^*$ becomes:

$$\dot{h}^* = V \sin\gamma + c_\gamma \left[2\omega_{cb} V + \frac{V^2}{R} \cos\gamma + \omega_{cb}^2 R \cos\gamma - g\cos\gamma + \frac{L}{m}\cos\sigma \right] + c_\gamma \gamma \left[\omega_{cb}^2 R \sin\gamma - g\sin\gamma - \frac{D}{m} \right] \tag{6}$$

B. Path Constraints

During re-entry the vehicle will encounter several kinds of loads. These loads are usually not allowed to exceed certain values, *i.e.,* the *flight-path constraints*. Two flight-path constraints are considered, *i.e.,* the heat flux and the *g-load*. For the heat flux q_c the (cold-wall) Chapman model is used as a first approximation:

$$q_c = \frac{c_1}{\sqrt{R_N}} \sqrt{\frac{\rho}{\rho_0}} \left(\frac{V}{V_c} \right)^{c_2} \tag{7}$$

with $c_1 = 1.06584{\cdot}10^8$ W/m^3/2, R_N = nose radius = 0.238 m, ρ = atmospheric density (kg/m^3), ρ_0 = density at sea level = 1.225 kg/m^3, V_c = circular velocity at re-entry = 7,905 m/s, and $c_2 = 3$.

The *g-load* n_g is defined to be the normalised acceleration due to the aerodynamic forces, drag, $D = C_D \bar{q} S_{ref}$, and lift, $L = C_L \bar{q} S_{ref}$, *i.e.,*

$$n_g = \frac{\sqrt{D^2 + L^2}}{m g_0} = \bar{q} S_{ref} \frac{\sqrt{C_D^2 + C_L^2}}{m g_0} \tag{8}$$

where m is the vehicle mass and $g_0 = 9.81$ m/s^2 is the standard gravitational acceleration on the Earth's surface. The dynamic pressure is defined as $\bar{q} = \frac{1}{2}\rho V^2$.

Inspecting Eqs. (7) and (8) more closely, we see that the predominant state dependency is on velocity and altitude. From Eq. (1) it is clear that $\dot{V}$ has a direct link with the angle of attack through the drag force. However, since h is a kinematic equation there is no direct coupling with the aerodynamic forces, and, as explained in he previous section, the pseudo-altitude was introduced. This variable can be changed by both angle of attack and bank angle. This relation is immediately clear from the formulation of the state-space system, which has been provided in Appendix A. Depending on the application, both α and σ can be used as guidance commands, either individually or as a combination. In the current study, σ is chosen, because changing α too much from its nominal value would affect the flight range that is maximal when flying at and angle of attack that provides the maximum lift-to-drag ratio.

For the tracking guidance to be developed both first and second time derivative will be required; for the heat flux $\dot{q}_c$ is found to be:

$$\dot{q}_c = \frac{c_1}{\sqrt{R_N}} \left(\frac{1}{2\sqrt{\rho}} \frac{\mathrm{d}\rho}{\mathrm{d}t} V^{c_2} + c_2 \sqrt{\rho} V^{c_2 - 1} \frac{\mathrm{d}V}{\mathrm{d}t} \right) \tag{9}$$

The time derivative of density can be rewritten as $\frac{\mathrm{d}\rho}{\mathrm{d}t} = \frac{\mathrm{d}\rho}{\mathrm{d}h}\frac{\mathrm{d}h}{\mathrm{d}t}$, such that the time dependency can be replaced by an altitude dependency; $\dot{h} = V\sin\gamma$ is known as the kinematic altitude equation, Eq. (3). Of course, $\frac{\mathrm{d}\rho}{\mathrm{d}h}$ could be obtained numerically, but for the sake of the discussion – and actually quite common to do so for guidance-law development – an exponential atmosphere is assumed. Thus:

$$\rho = \rho_0 e^{-\frac{h}{H_s}} \qquad \Rightarrow \qquad \frac{\mathrm{d}\rho}{\mathrm{d}h} = -\frac{\rho}{H_s} \tag{10}$$

such that

$$\frac{\mathrm{d}\rho}{\mathrm{d}t} = \frac{\mathrm{d}\rho}{\mathrm{d}h}\frac{\mathrm{d}h}{\mathrm{d}t} = -\frac{\rho}{H_s}\dot{h} \tag{11}$$

With a little effort the second derivative is obtained in a similar manner. The time derivative of the first term in brackets of Eq. (9) is given by

$$\frac{\mathrm{d}}{\mathrm{d}t}\left(\frac{1}{2\sqrt{\rho}}\frac{\mathrm{d}\rho}{\mathrm{d}t}V^{c_2}\right) = -\frac{1}{4\rho\sqrt{\rho}}\dot{\rho}^2 V^{c_2} + \frac{1}{2\sqrt{\rho}}\ddot{\rho}V^{c_2} + \frac{1}{2\sqrt{\rho}}\dot{\rho}V^{c_2-1}\dot{V} \tag{12}$$

and the second term

$$\frac{\mathrm{d}}{\mathrm{d}t}\left(c_2\sqrt{\rho}V^{c_2-1}\frac{\mathrm{d}V}{\mathrm{d}t}\right) = c_2\frac{1}{2\sqrt{\rho}}\dot{\rho}V^{c_2-1}\dot{V} + c_2\sqrt{\rho}V^{c_2-2}\dot{V}^2 + c_2\sqrt{\rho}V^{c_2-1}\ddot{V} \tag{13}$$

For $\ddot{\rho}$ it is found that

$$\frac{\mathrm{d}}{\mathrm{d}t}\left(\frac{\mathrm{d}\rho}{\mathrm{d}t}\right) = \frac{\mathrm{d}}{\mathrm{d}t}\left(\frac{\mathrm{d}\rho}{\mathrm{d}h}\frac{\mathrm{d}h}{\mathrm{d}t}\right) = \frac{\mathrm{d}^2\rho}{\mathrm{d}h^2}\dot{h}^2 + \frac{\mathrm{d}\rho}{\mathrm{d}h}\ddot{h} \tag{14}$$

with

$$\frac{\mathrm{d}\rho}{\mathrm{d}h} = -\frac{\rho}{H_s} \qquad \text{and} \qquad \frac{\mathrm{d}^2\rho}{\mathrm{d}h^2} = \frac{\rho}{H_s^2} \tag{15}$$

Note that the above second density derivative is not that important, considering that it evaluates to a term on the order of 10^{-10} and even much smaller in the region of interest. The second derivatives $\ddot{V}$ and $\ddot{h}$ could be derived analytically from the equations of motion, but this would lead to additional large expressions. For now, we will therefore get these derivatives by numerically differentiating the first-order derivatives.

Equivalent expressions can be derived for $\frac{\mathrm{d}n_g}{\mathrm{d}t}$ and $\frac{\mathrm{d}^2n_g}{\mathrm{d}t^2}$, the result of which is simply stated below.

$$\dot{n}_g = \left(\frac{1}{2}\dot{\rho}V^2 + \rho V\dot{V}\right)S_{ref}\frac{\sqrt{C_D^2 + C_L^2}}{mg_0} \tag{16}$$

$$\ddot{n}_g = \left(\frac{1}{2}\ddot{\rho}V^2 + 2\dot{\rho}V\dot{V} + \dot{\rho}\dot{V}^2 + \rho V\ddot{V}\right)S_{ref}\frac{\sqrt{C_D^2 + C_L^2}}{mg_0} \tag{17}$$

where it has been assumed that C_D and C_L vary only slowly compared to V and h, and have been assumed constant while establishing the derivatives. Obviously, one can update the coefficients with their actual values whenever the derivatives are evaluated. The individual derivatives appearing in the above equations have been discussed above.

The way the above equations will be used in the tracking law is as follows. Let us define the heat-flux error as $\Delta q_c = q_{c,setpoint} - q_c$. Once the setpoint is reached, the error should remain zero, so the desired heat-flux rate is $\dot{q}_{c,des} = 0$, implying that the corresponding error is $\Delta\dot{q}_c = \dot{q}_{c,des} - \dot{q}_c = -\dot{q}_c$. For all practical purposes, the errors can be assumed small, such that the error dynamics can be described by a linear state-space model. To gain insight in the relation between the states (ΔV and Δh^*), controls ($\Delta\alpha$ and $\Delta\sigma$), and the outputs (Δq_c and Δn_g), in Appendix A such a model is briefly reviewed. This model will also be used while formulating the NDI tracking law in Sec. III.B, as one of the requirements is that the dynamics model is affine in its control.

III. Guidance

A. Nominal Guidance

To limit the mass of the TPS an optimal trajectory that minimises the total integrated heat load should be flown, which effectively means that the heat-flux constraint should be tracked for as long as possible. At the same time, the maximum allowable mechanical load should be observed. It was found in Ref. 7 that tracking these constraints could be combined in a single guidance law, *i.e.*, ρV^n = constant. Here, $n = 2$ for the mechanical load, defined by the dynamic pressure, see Eq. (8), and $n = 6$, which defines the proportionality of q_c^2, see Eq. (7). This part of the guidance constitutes the nominal guidance, and will briefly be discussed here. The tracking guidance, responsible for reducing deviations from the nominal trajectory to zero, will be presented in the next section.

The entry begins with the vehicle in maximum lift configuration, which, for all practical purposes, means to fly with the largest possible commanded angle of attack (for this vehicle: $\alpha_c = 45°$). This yields the lowest maximum heat flux. This peak value may be larger than the set point that should be tracked, as it is depending on entry conditions, vehicle mass, and aerodynamic characteristics. For given parameters, this peak flux is a given that cannot be affected. The actual set point for heat-flux tracking is usually lower, here it is set at $q_{c,max} = 1700$ kW/m^2, and the first time after the peak this value is reached, the guidance system is activated. The bank angle will be commanded to track the constraint, whereas the angle of attack is reduced to the one for maximum L/D configuration to increase manoeuvrability and flight range (*Hyperion-1*: $\alpha_c = 20°$).

From the condition ρV^n = constant it follows that:

$$\frac{\mathrm{d}(\rho V^n)}{\mathrm{d}t} = \frac{\mathrm{d}\rho}{\mathrm{d}h}\dot{h}V^n + n\rho V^{n-1}\dot{V} = 0 \tag{18}$$

Substituting the formulation of exponential atmosphere, Eq. (10), as well as the equations of motion Eqs. (1) (ignoring the small centrifugal-acceleration term) and (3), yields:

$$-\frac{\rho}{H_s}V^{n+1}\sin\gamma - n\rho V^{n-1}\left(\frac{c_n}{2KV^{n-2}} - g\sin\gamma\right) = 0 \tag{19}$$

with $K = \frac{m}{C_D S_{ref}}$ being the ballistic coefficient (kg/m^2). Isolating the flight-path angle, γ, it can be treated as a "commanded" value that fulfils the tracking criterion:

$$\sin\gamma_c = -c_n \frac{n}{V^{n-2}} \frac{H_s}{2K} \frac{1}{V^2 - ngH_s} \tag{20}$$

with $c_n = \rho V^n$ = constant and $H_s = 7{,}050$ m being the scale height.

To link the above equation to the commanded bank angle, $\sigma_{0,c}$, as shown in Eq. (2), we will establish the relation $\dot{\gamma} = \frac{\mathrm{d}\gamma}{\mathrm{d}V}\frac{\mathrm{d}V}{\mathrm{d}t}$. So, from Eq. (2) it follows, while retaining the accelerations due to the rotation of the Earth to minimise the deviation from the actual flight path (in particular the Coriolis acceleration cannot be ignored):

$$V\left.\frac{\mathrm{d}\gamma}{\mathrm{d}t}\right|_c = \frac{L\cos\sigma_{0,c}}{m} + \sum(a_\gamma)_i \tag{21}$$

with $\sum_i (a_\gamma)_i$ being the sum of all acceleration terms other than the vertical-lift acceleration:

$$\sum_i (a_\gamma)_i = -g\cos\gamma_c + 2\omega_{cb}V\cos\delta\sin\chi + \frac{V^2}{R}\cos\gamma_c + \omega_{cb}^2 R\cos\delta(\cos\delta\cos\gamma_c + \sin\gamma_c\sin\delta\cos\chi) \tag{22}$$

Isolating the bank angle yields:

$$\cos\sigma_{0,c} = \frac{m}{L}\left[\left.\frac{\mathrm{d}\gamma}{\mathrm{d}t}\right|_c - \sum_i (a_\gamma)_i\right] = \frac{m}{L}\left[\left.\frac{\mathrm{d}\gamma}{\mathrm{d}V}\right|_c \dot{V} - \sum_i (a_\gamma)_i\right] \tag{23}$$

The derivative of Eq. (20) with respect to velocity, $\left.\frac{\mathrm{d}\gamma}{\mathrm{d}V}\right|_c$, yields:

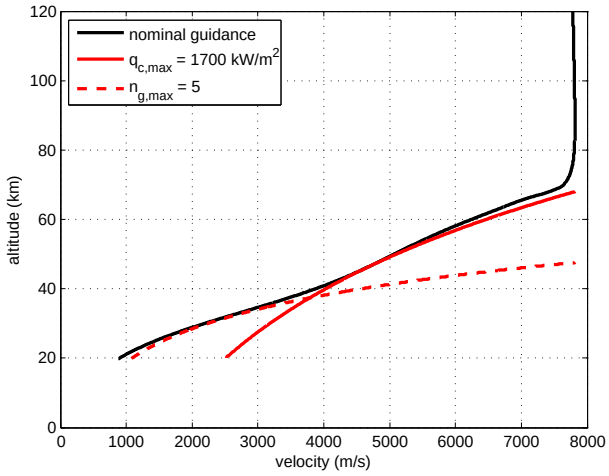

Figure 2. *Hyperion-1* **reference trajectory in relation to its path constraints.**

$$\left.\frac{\mathrm{d}\gamma}{\mathrm{d}V}\right|_c = \frac{c_n}{\cos\gamma_c}\left\{\frac{2n^2KH_s(V^{n-1}+gH_s(n-2)V^{n-3})}{[2KV^{n-2}(V^2+gnH_s)]^2}\right\} \tag{24}$$

with $\dot{V}$ given by Eq. (1).

Inspecting the guidance law Eq. (23) shows that reference commands for both $\dot{\gamma}_c$ and γ_c are required. The latter may be different from the actual γ, due to uncertainties in environment or vehicle characteristics, and to compensate for this difference a small correction term, $\Delta\dot{\gamma}_c$, may be added to $\dot{\gamma}_c$, given by Eq. (21). With $e_\gamma = \gamma_c - \gamma$ being the error in γ, a PID compensator in the form of

$$\Delta\dot{\gamma}_c = K_{\gamma p}e_\gamma + K_{\gamma i}\int_0^t e_\gamma dt + K_{\gamma d}\frac{\mathrm{d}e_\gamma}{\mathrm{d}t} \tag{25}$$

can serve that purpose.

Finally, to avoid any jumps in guidance command due to discrete changes in the input some smoothing filters are included in the guidance loop:

1. At the transition from q_c = constant to n_g = constant, the coefficient n is adapted and thus also the tracking constant $c_n = \rho V^n$, by applying a smooth step function,[8]

2. Additional damping is provided in case c_n changes rapidly by applying a simple PD regulator on the (normalised) c_n,[8] and

3. To avoid abrupt changes in $\Delta\alpha_c$ and $\Delta\sigma_c$ due to a rapid increase in *g-load* towards the end of heat-flux tracking, a smooth decrease to zero in heat-flux error is enforced, when q_c has reached a value smaller than 90% of the set point.[9]

To conclude the discussion on the nominal guidance, Fig. 2 shows the reference entry trajectory in relation to the two constraints heat flux and *g-load*.

B. Non-linear Dynamics Inversion

The fundamental concept of INDI is formulated as follows. Let us assume a non-linear system, affine in its control:

$$\dot{\mathbf{x}} = \mathbf{f}(\mathbf{x}) + \mathbf{G}(\mathbf{x})\mathbf{u} \tag{26}$$

where $\mathbf{f}(\mathbf{x})$ represents the system dynamics, $\mathbf{G}(\mathbf{x})$ is the state-dependent control matrix of dimension $n \times m$, and $\mathbf{u}$ is the $m \times 1$ control vector. To get the approximated dynamics in its incremental form, the first-order Taylor-series expansion of $\dot{\mathbf{x}}$, evaluated around $[\mathbf{x_0}, \mathbf{u_0}]$ is

$$\dot{\mathbf{x}} = \dot{\mathbf{x}}_\mathbf{0} + \underbrace{\frac{\partial}{\partial \mathbf{x}} \left[\mathbf{f}(\mathbf{x}) + \mathbf{G}(\mathbf{x})\mathbf{u}\right]\Big|_{\substack{\mathbf{x}=\mathbf{x_0} \\ \mathbf{u}=\mathbf{u_0}}}}_{\mathbf{F}(\mathbf{x_0},\mathbf{u_0})=\mathbf{F_0}} (\mathbf{x} - \mathbf{x_0}) + \underbrace{\frac{\partial}{\partial \mathbf{u}} \left[\mathbf{G}(\mathbf{x})\mathbf{u}\right]\Big|_{\substack{\mathbf{x}=\mathbf{x_0} \\ \mathbf{u}=\mathbf{u_0}}}}_{\mathbf{G}(\mathbf{x_0})=\mathbf{G_0}} (\mathbf{u} - \mathbf{u_0}) \tag{27}$$

For a sufficiently high control update (and thus small time increment), $\mathbf{x}$ approaches $\mathbf{x_0}$, so $\mathbf{F_0}(\mathbf{x} - \mathbf{x_0}) << \mathbf{G_0}(\mathbf{u} - \mathbf{u_0})$ and can thus be ignored. The linearised system $\boldsymbol{\nu} = \dot{\mathbf{x}}$ is rewritten as

$$\boldsymbol{\nu} = \dot{\mathbf{x}}_\mathbf{0} + \mathbf{G_0}\delta\mathbf{u} \tag{28}$$

where the control *increment* $\delta\mathbf{u} = \mathbf{u} - \mathbf{u_0}$ has been introduced. This increment is obtained by inverting Eq. (28), and is to be added to the nominal (or reference) control $\mathbf{u_0}$ to obtain the control $\mathbf{u}$, input to the non-linear system. So

$$\mathbf{u} = \mathbf{u_0} + \delta\mathbf{u} = \mathbf{u_0} + \mathbf{G_0}^{-1}\left[\boldsymbol{\nu} - \dot{\mathbf{x}}_\mathbf{0}\right] \tag{29}$$

In case we want to track a heat-flux profile Eq. (7), with $\dot{q}_c = 0$ and the "control" given by $\Delta\sigma$, we begin as follows. From the discussion in Sec. II.B and Appendix A we can assume that $\Delta\mathbf{y}$, $\Delta\dot{\mathbf{y}}$, and $\Delta\ddot{\mathbf{y}}$ are known and available, either from analytical expressions or numerical differentiation. Equation (27) is rewritten as:

$$\dot{\mathbf{y}} = \dot{\mathbf{y}}_\mathbf{0} + \Delta\dot{\mathbf{y}} = \mathbf{A}^*\Delta\mathbf{x} + \mathbf{B}^*\Delta\mathbf{u} \tag{30}$$

because for tracking $\dot{\mathbf{y}}_\mathbf{0} = \mathbf{0}$ (the steady-state condition), and $\Delta\dot{\mathbf{y}}$ has been rewritten with the aid of Eq. (A16). Thus, Eq. (28) becomes

$$\boldsymbol{\nu} = \mathbf{B}^*\delta\mathbf{u} \tag{31}$$

and is thus no longer an *incremental* guidance law, but a form of non-linear dynamics inversion.

For the remainder of this section, it is assumed that there are separate tracking laws for either heat flux or *g-load*, where only the former will be detailed here. The control-law design is based on outer-loop control of the heat-flux error, $\Delta y = q_{c,setpoint} - q_c$, and inner-loop control of its first derivative, $\Delta\dot{y} = \dot{q}_{c,setpoint} - \dot{q}_c = -\dot{q}_c$. So, for the outer loop

$$y_{out} = \Delta y \tag{32}$$

with the generic formulation for its derivative given by

$$\dot{y}_{out} = \nu_{out} = \Delta\dot{y} = \dot{q}_{c,setpoint} - \dot{q}_c \tag{33}$$

The desired heat-flux rate, *i.e.,* the transition rate that in the end should lead to the steady-state condition $\dot{q}_{c,setpoint} = 0$, is easily obtained from the above equation through

$$\dot{q}_{c,des} = \nu_{out} + \dot{q}_c \tag{34}$$

with

$$\nu_{out} = K_{p,out}\Delta y + K_{d,out}\Delta\dot{y} \tag{35}$$

which may be obtained from a simple PID control law; in the current application we will start with proportional and derivative control.

To design the inner-loop control, we start with the inner-loop output vector:

$$y_{in} = \Delta\dot{y} \tag{36}$$

with its derivative, $\Delta\ddot{y}$, given by Eq. (A18), or, equivalently, Eqs. (12) and (13). Let us further define $\dot{y}_{in} = \Delta\ddot{y} = \nu_{in}$. The virtual control parameter, ν_{in}, may yet again be obtained from a simple P(ID) control law.

$$\nu_{in} = K_{p,in}\dot{q}_{c,e} = K_{p,in}\left(\dot{q}_{c,des} - \dot{q}_c\right) = K_{p,in}\nu_{out} \tag{37}$$

with $\dot{q}_{c,des}$ following from the outer-loop control. Substituting ν_{in} into the equivalent of Eq. (29), finally, will give the bank-angle tracking command:

$$\delta\sigma = (B^*)^{-1}\left[\nu_{in} - \ddot{q}_c\right] \tag{38}$$

where for now, as stated in Section II.B, $\ddot{q}_c$ follows from numerical differentiation.

Due to the number of design parameters in both the nominal and the tracking guidance, and taking transition effects of the complete trajectory into account, makes tuning the design parameters of the guidance system quite laborious. Even when freezing the nominal guidance parameters, finding the optimal combination of inner-loop and outer-loop gains proved to be a tedious task, partially due to the relatively long run times (mission duration on the order of 1000 s, and a guidance sample frequency of 50-100 Hz).

For the outer-loop gains we select $K_{p,out}$ = -1.16·10^{-4}, the corresponding derivative gain is $K_{d,out} = 10K_{p,out}$. The inner-loop gain is $K_{p,in} = 100$. It is noted that during the tuning process, both a PID and PD law for the outer and inner loop, respectively, were studied. It appeared that adding extra terms made it harder to tune the tracking system, and will only be pursued at a later stage. Finally, a maximum bank rate of $\dot{\sigma}_c = 15°/\text{s}$ will be used, and to avoid rather discrete changes in command, a shaping filter is applied to σ_c. The transfer function of this command shaper is given by

$$H_c(s) = \frac{1}{\tau s + 1} \tag{39}$$

with time constant $\tau = 2.5$ s.

IV. Results

A. Preliminary Analysis

This section will provide the results of the preliminary analysis done for the combination of nominal guidance, Sec. III.A, and the tracking guidance, Sec. III.B. For the sake of comparison, the first run will be done with only the nominal guidance. The resulting heat-flux and *g-load* constraint values are shown in Fig. 3. The heat-flux constraint is tracked for about 500 s, after which the guidance system cannot keep up with the rapidly changing conditions. One can also see this in the plot for the *g-load*, which rapidly increases after $t = 600$ s. However, with the peak value of just over 4 g, there is no need for additional tracking. To anticipate on future trajectory optimisation the integrated heat load, Q, and flight range, d_{tot} have been plotted as well. These objectives are typically conflicting, as Q should be minimised, yielding a minimum thermal-protection system mass, and the flight range maximised, to improve the manoeuvrability. Final values are $Q = 1318$ MJ/m^2 and $d_{tot} = 6018$ km. Figure 4 shows the corresponding guidance commands, angle of attack (commanded as openloop values) and the bank angle. The dip in σ_c around $t \approx 700$ s is caused by the pre-activation of the *g-load* tracking law, at 20% of the *g-load* set point of 4.8. At times, the bank angle is commanded to values larger than 90°, implying a lift-down orientation. A lift-up orientation at those moments would lead to constraint violations.

The second run is aimed at getting a feel for the capabilities of the tracking system. In Fig. 5 the performance of the tracking guidance system can clearly be seen. The heat flux is tracked for 200 s longer, reducing the heat load by some 30 MJ/m^2 to $Q = 1289$ MJ/m^2. The maximum *g-load* is not affected by this. The longer tracking does affect the flight range, which is reduced by some 200 km to $d_{tot} = 5827$ km. The change in performance may not seem large, but it is also not the only aspect of importance. Also the robustness in the presence of uncertainties is a design priority, which will be studied shortly. To conclude this part, the corresponding bank-angle command is shown in Fig. 6. At first sight, the profile looks less than optimal. This may be true, if one realises that at the moment the oscillations start, there is an internal switch to *g-load* tracking, and, as a consequence, a rapid change in operational conditions. So, not only the tracking guidance should be optimised, also the nominal guidance has to be reviewed with robustness in mind. In the next section this will be addressed in some more detail.

B. Review of the Nominal System

To understand in which direction a redesign of the guidance system has to go, two aspects are reviewed: 1) transition of heat-flux to *g-load* tracking, at (currently) 20% of the *g-load* set point, and 2) extension of the heat-flux tracking towards the end of the profile. Figure 7 shows two simulations, run with nominal

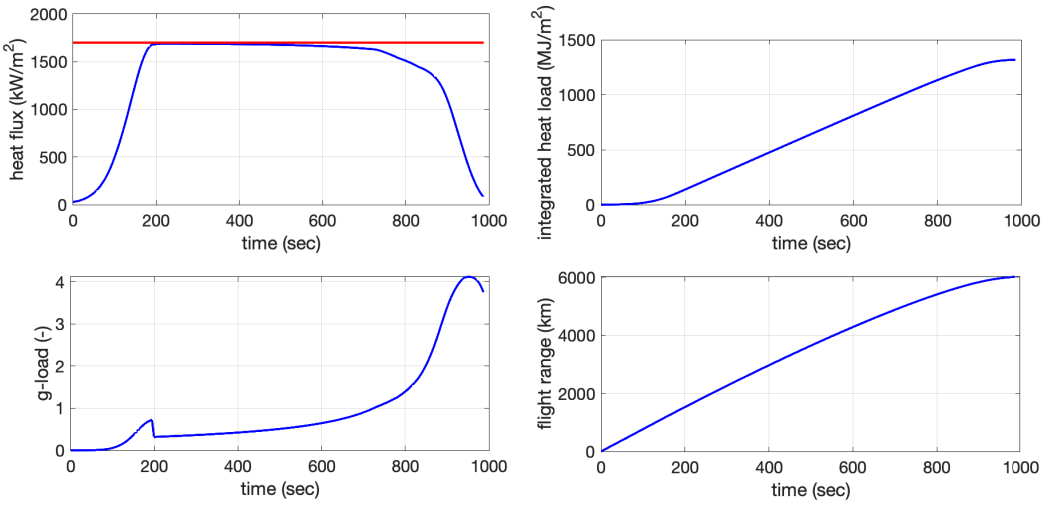

Figure 3. *Hyperion-1* **reference trajectory flown with nominal guidance.**

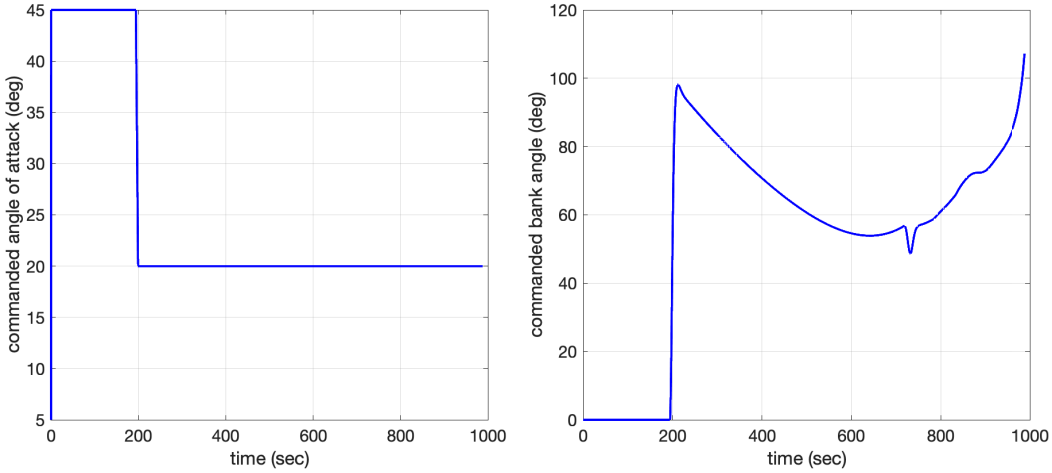

Figure 4. *Hyperion-1* **nominal guidance commands.**

guidance only. The one simulation is the default one with a *g-load* set point of 4.8, whereas the other has no constraint on the *g-load*. One can observe from the left figure that the switch at 20% is really necessary, as the *g-load* starts rising rapidly soon after, and with a later switch the vehicle would not be able to respond quickly enough to avoid constraint violation. The unconstrained flight shows a peak *g-load* of about 24 g. The bank-angle profile on the right confirms that the transition from heat-flux to *g-load* tracking is not smooth enough, despite the smoothener step function applied to the transition value of n, going from 6 down to 2. The bank-angle profile for the unconstrained case is very smooth, even though it progresses to a full lift-down orientation. To understand this one needs to realise that in this case only the heat-flux tracking is in operation. When both trackings are active the heat-flux set point cannot be tracked beyond $t \approx 600$ s, when the transition is initiated, as can be seen in Fig. 3. When this limitation is gone the nominal guidance provides an extended bank-angle command that corresponds best to flying along the heat-flux constraint. However, in doing so the bank angle has to become so large to enter into a steep dive to sustain the setpoint value of $\rho V^6 = \text{constant}$.

The effect of extended heat-flux tracking is clearly indicated in Fig. 8. For the regular dual-constraint tracking, the extension of heat-flux tracking towards the end of the heat-flux plateau resulted in the additional bank-angle oscillations shown earlier in Fig. 6. A similar effect is observed when there is no *g-load* constraint and the heat-flux tracking is prolonged, even without this forced extension (see the red line in Fig. 8).

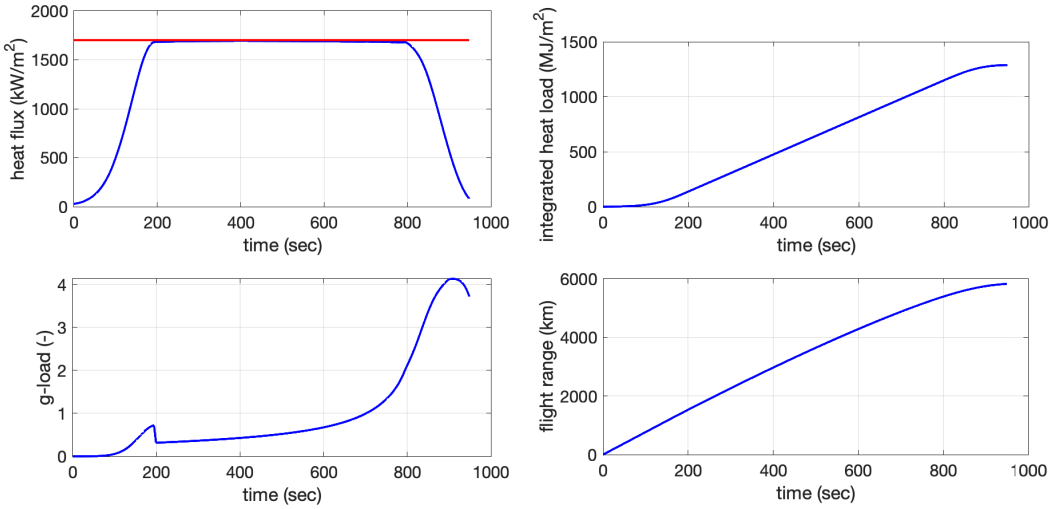

Figure 5. *Hyperion-1* **reference trajectory flown with nominal and tracking guidance.**

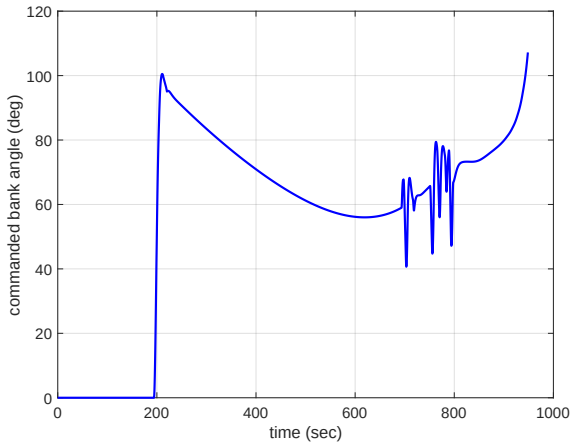

Figure 6. *Hyperion-1* **bank-angle command.**

Removing the forced extension and re-introducing the constraint yields a much smoother bank-angle profile, more or less comparable to the nominal bank angle shown in Fig. 7. Obviously, this goes at the expense of a drop in tracking performance (and thus also a slight increase in integrated heat load), but to avoid attitude oscillations and risking the vehicle's stability, this is worth it.

It is clear from this analysis, though, that the nominal guidance should be reviewed. The transition from heat-flux to *g-load* tracking should be made even smoother to avoid the rather abrupt changes in commanded bank angle. High-gain tracking systems do not always deal well with these abrupt changes, and the way the NDI tracking guidance has currently been set up, using the tracking error and its derivatives as input, has made it indeed sensitive to these changes (most notably visible in the higher-order derivatives). For now, the nominal guidance will be used as is, and the focus will be on the tracking capabilities of the NDI system. This will be explored in the next section through sensitivity analysis.

C. Sensitivity Analysis of the Tracking System

Focussing on the tracking guidance for now, a (limited) sensitivity analysis is performed. To be able to judge the performance, the LQY tracking system developed earlier[8,9] is used as baseline. This LQY is an output feedback guidance system, centred around linearised dynamics of velocity and pseudo altitude (see the appendix for the state-space model); taking the heat-flux error as input the output is a corrective

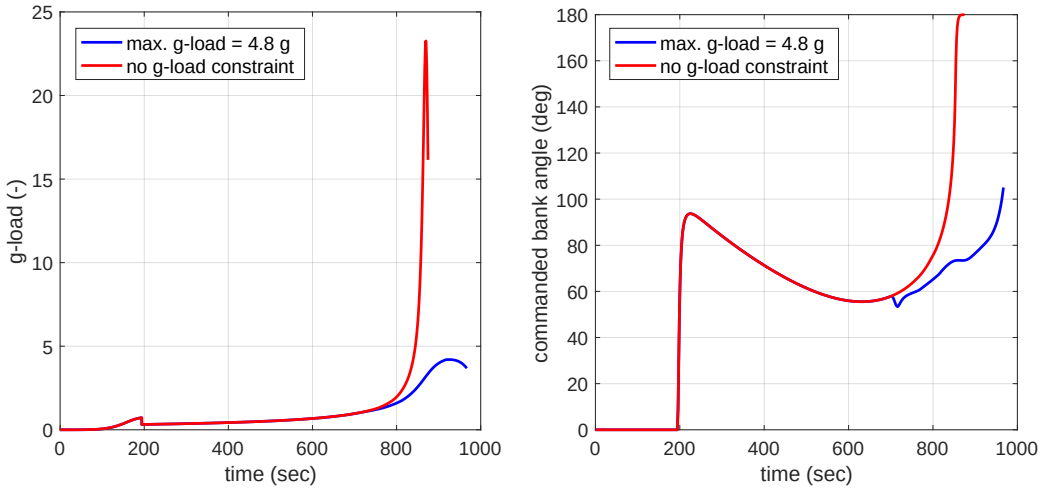

Figure 7. The effect of the *g-load* constraint on the nominal guidance command.

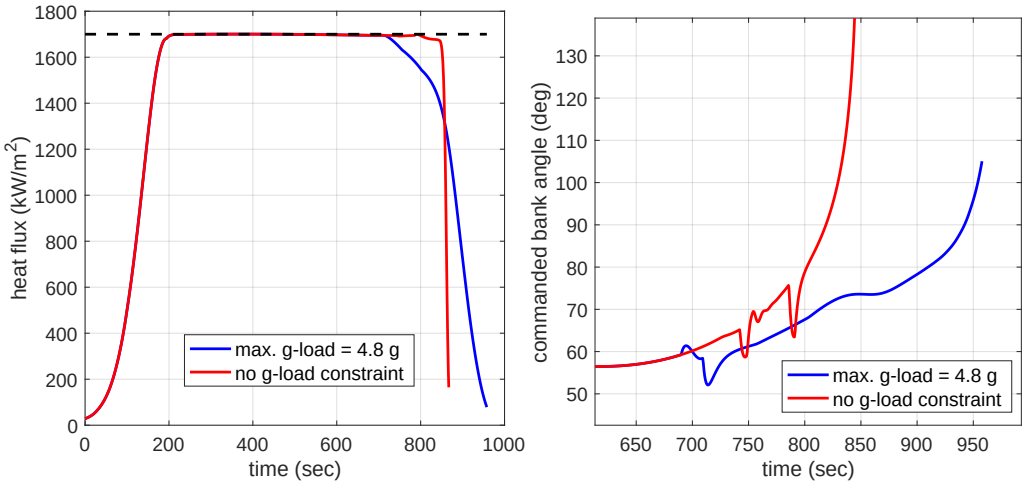

Figure 8. The effect of the *g-load* constraint on the tracking guidance command.

bank angle. A first batch of Monte-Carlo simulations will be executed, with $N = 250$ runs. The applied uncertainties are in the vehicle mass ($\Delta m = \pm$ 20 kg), the atmospheric density ($\Delta\rho = \pm$ 25%), the speed of sound ($\Delta a = \pm$ 10%), the drag and lift coefficient (ΔC_D, $\Delta C_L = \pm$ 10%), and the initial states velocity and flight-path angle ($\Delta V_0 \pm$ 100 m/s , $\Delta\gamma_0 \pm 0.1^\circ$), each with a uniform distribution. It is noted that the combination of a large density error in combination with large initial-state errors will be particularly demanding on the guidance system as a whole.

The performance of the tracking system can be judged using several performance indices. The first one is the integrated heat load, Q, which should be as low as possible. Because this is achieved by flying along the heat-flux constraint, the second performance index is the integrated heat-flux deviation from this constraint. Mathematically this index is defined as

$$\sum_{q_{c,err}} = \int_{t_1}^{t_2} \sqrt{(q_c - q_{c,max})^2}\mathrm{d}t \tag{40}$$

with t_1 and t_2 the activation and de-activation time of the heat-flux tracking. This index has been visualised in Fig. 9, where the shaded area corresponds with Eq. (40). The corresponding guidance effort can be represented by the integrated bank angle over time. Here, the total guidance effort is considered, *i.e.,*

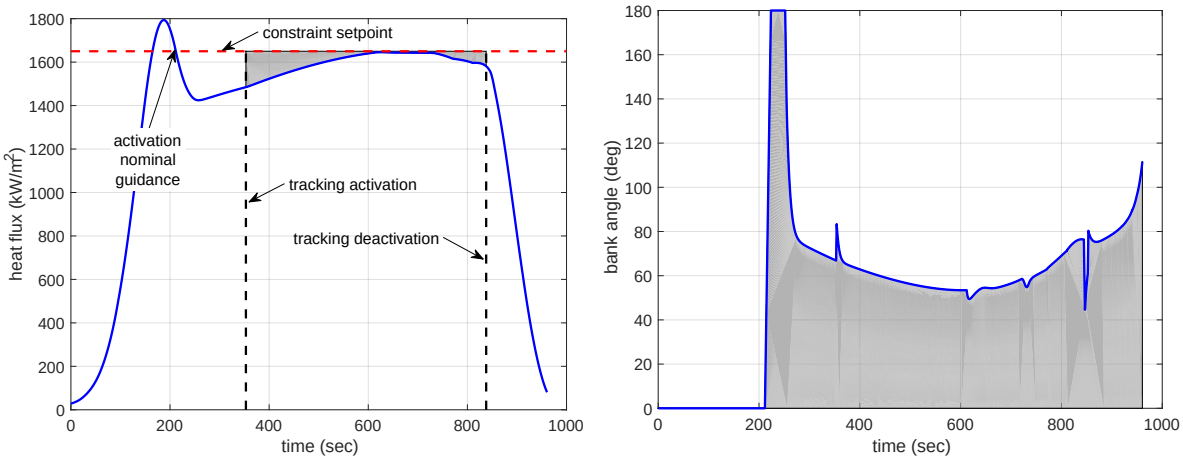

(a) heat-flux error (b) guidance effort

Figure 9. Sample integrated performance indices, represented by the shaded areas.

the summation of nominal and tracking command, because the nominal guidance command is in principle affected by the tracking and should therefore be taken into account. This index is thus defined as:

$$\sum_{\sigma} = \int_{0}^{t_{final}} \sigma_c \mathrm{d}t \tag{41}$$

It is obvious that the above metrics should be as small as possible. For good measure, also the peak value of q_c will be observed, and in light of the earlier discussion on bank-angle oscillations an additional metric will be defined to cover this.

To detect oscillations or otherwise discrete changes in a parameter controls, the cumulative moving standard deviation can be used. For a subset j of n_s out of a total of N samples of an arbitrary signal u, the moving mean is defined as $\bar{y}_j = \frac{1}{n_s} \sum_{i=j}^{j+n_s-1} u_i$. Here, j will run from $j = 1+n_s/2$ to N-$n_s/2$, so each subsequent subset will shift by only one sample. Let the squared deviation from this mean be defined as $s_{u,j} = (u_{j+n_s/2} - \bar{y}_j)^2$, which represents the value at the midpoint of subset j. The cumulative standard deviation, F_u, for subset j is then

$$F_{u_j} = \sqrt{\frac{1}{N - n_s - 1} \sum_{k=1}^{j} s_k} \tag{42}$$

It is stressed that even a rapid change of bank angle, as is apparent when the nominal guidance is activated, will contribute to the oscillation index. One should thus not use this index as the absolute truth, but more as a way of comparing different situations. It is left as future work to properly deal with these oscillations.

To begin the analysis with the integrated heat load, a variation of about ± 15% around the nominal value was observed, with a similar performance of both tracking systems (a slight advantage for the NDI tracking system is seen). Given the large uncertainties that were simulated this does not seem to be a bad result. It should be noted, though, that this variation is not just the functioning of the tracking system. Due to the variation in the initial state, part of the trajectories will result in a peak value of heat flux that cannot be lowered by any guidance system. For a given entry state, vehicle mass, nose radius, and aerodynamic configuration , the maximum peak value can only be reduced if the vehicle lift can be increased by further increasing the angle of attack. The current angle of attack is 45°, and considered to be a safe maximum. Thus, keeping this α_c fixed, means that some trajectories will experience a larger peak value than the setpoint, and heat-flux tracking is only activated when the flux has reduced from this peak value to the setpoint, see also Fig. 9. Obviously, this overshoot will increase the integrated heat load.

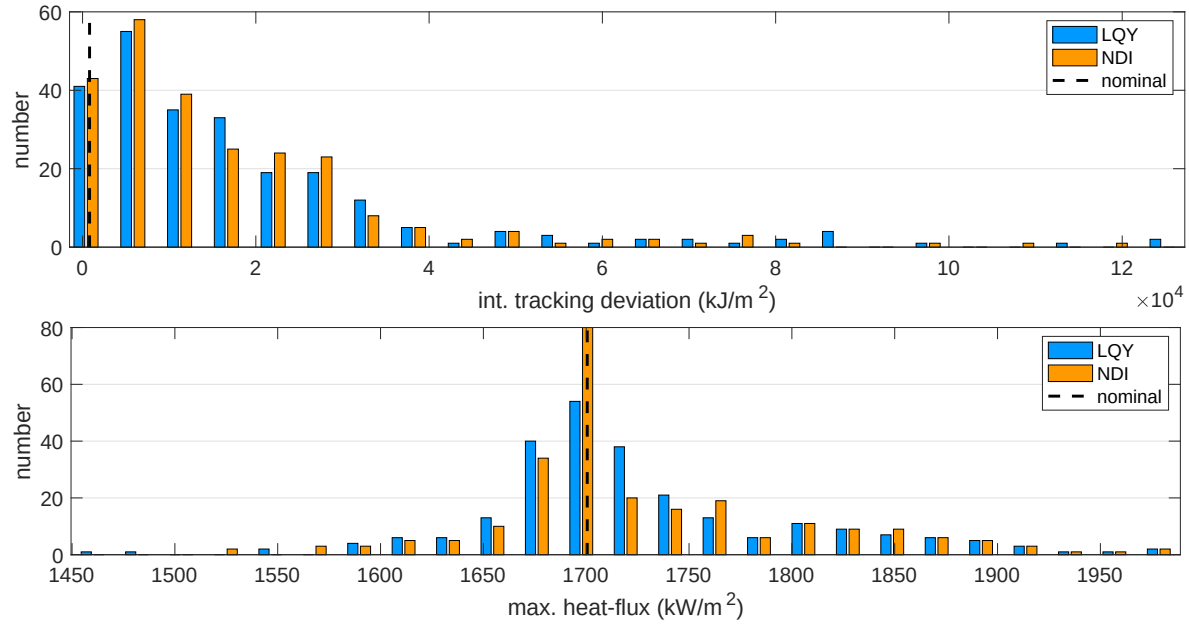

Figure 10. Integrated tracking error and maximum heat flux (Monte-Carlo simulation with 250 runs).

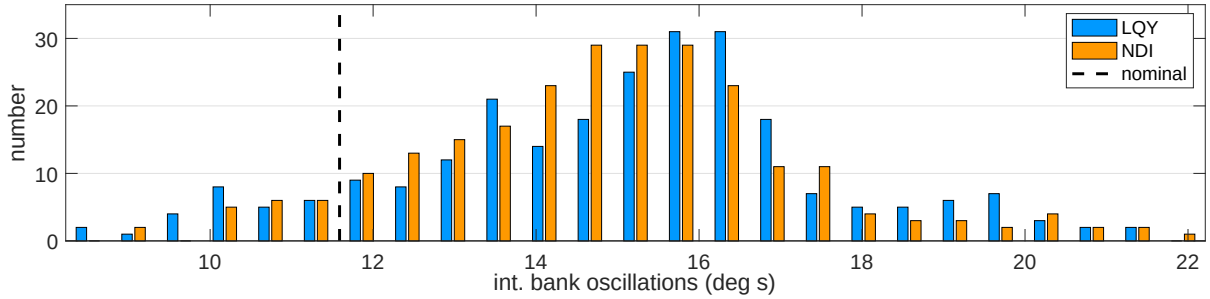

Figure 11. Integrated bank-angle oscillations (Monte-Carlo simulation with 250 runs).

Figure 10 does show the tracking-system's performance. Because the seemingly large spread of the deviations, in particular in relation to the nominal value, the performance may seem not so great. This is not altogether true, though, because due to the errors in aerodynamics and atmospheric density, the heat flux stays often *under* the setpoint (this is especially true for the large outliers), and not as much *over* it. In that sense, the tracking could be better, but the vehicle's integrity is not jeopardised, which is a major objective of the guidance system. It should be noted, though, that extending the tracking system with some form of integral-error control will improve the tracking, as currently such integral control has not been added. Comparing the two tracking systems, shows a slight favour to the NDI tracking system.

In the second plot, the maximum heat flux is shown, and confirms the earlier discussion on initial overshoot due to limited vehicle capabilities. For both tracking systems the overshoots of $q_c > 1.75$ MW/m^2 are the same, implying it is indeed the given trajectory. Overshoots below this value, but above or equal to the setpoint of 1.7 MW/m^2 shows a much better performance for the NDI: not only can it correct an overshoot sooner and thus reducing it, but it also manages to keep the maximum heat flux at the exact value of the setpoint in 40% more of the cases.

The last result shown here are the integrated bank-angle oscillations, see Fig. 11. Even though being an abstract performance index, it does show the relative comparison between the tracking systems on one hand, and between the perturbed cases and the nominal trajectory on the other. To begin with the latter, the nominal index is 11.6°s, corresponding to the plot shown in Fig. 8 (note that only the part where abrupt changes in σ_c occur is shown; the part before is the same as the one presented in Fig. 7). Analysis of

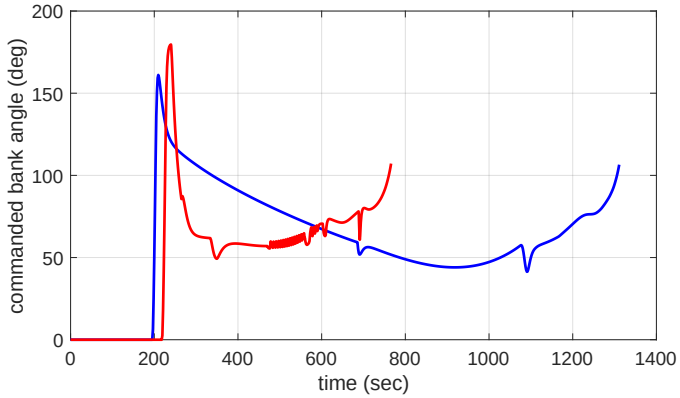

Figure 12. Two bank-angle profiles for similar values of the oscillation index (value of about 19°s).

this index is made difficult, as the index is depending on (obviously) the oscillations, abrupt non-oscillatory changes, and the flight duration. To visualise this, in Fig. 12 two bank-angle profiles are shown that have a similar oscillation index of about 19°s. The longer flight does not exhibit oscillations, but the shorter one does. Obviously, these oscillations need to addressed with an update of the design of the NDI tracking system, to begin with filtering the higher-order derivatives of the heat-flux error. Overall, the NDI does seem to have a lower oscillation index than the LQY.

Note that the integrated bank-angle effort as defined by Eq. (41) is very much dependent on the flight duration, which ranges from 766 to 1311 s. Obviously, the longer flights would show a much larger $\sum_{\sigma}$. It does make sense then to scale the found values by dividing them by the corresponding flight durations. For instance, for the nominal flight (with NDI tracking), the original value was $\sum_{\sigma} = 53{,}438°$s, and with a flight duration of $t_{final} = 958$ s, the scaled value is 55.8° (the unit changes, since the integration takes place over a normalised time interval). For the Monte-Carlo results, the original values showed a variation of -18% to +47% with respect to nominal. Scaling the index with flight time, gives the range -40% to +21%, which is much more favourable for the guidance-system performance (the LQY tracking guidance has a 1% wider range on either side). All in all, this bank-angle effort is no reason for concern, considering the large required bank angle to begin with. At initiation of the tracking the bank angle may spike to a (saturated) value of 180°, but this never lasts more than a few guidance samples. The bank angle never saturates later in the flight.

Before we come to the last batch of simulations, some explanation is in order. In previous work, the use of simple adaptive control as tracking guidance system was studied.[9] Despite its good performance, it was found to have a slower instantaneous response compared to a higher-gain LQY. It was then decided to combine the two tracking systems, having the nominal guidance and LQY acting as the stabilising inner-loop, and to have the adaptive tracking guidance serve as an outer-loop corrective guidance. This, to ensure minimum tracking error due to the integral component of the adaptive guidance law. Part of the on-going research, the same architecture is used now, where the NDI tracking guidance will be part of the outer loop (see Fig. 13). Note that the inner loop will be sampled at a lower frequency (50 Hz), to give the outer loop the time to "catch up" (at 100 Hz).

Running the same Monte-Carlo batch (identical initial seed for the random generator) for the new configuration, the results can now be compared with the previously obtained NDI tracking guidance (as it is the better tracking system compared to the LQY). It can easily be seen in Fig. 14 that combining the two tracking systems in an outer and inner loop does show some benefits. A further reduction of the tracking error is achieved, and also the maximum heat flux is more centred around the nominal value. The outliers are not included in this observation, as they are very similar for either tracking combination.

Summarised, it is safe to say that the application of the NDI tracking guidance offers potential, but of course more study is required, especially when the nominal guidance will be reviewed. Re-optimisation of the design parameters of the tracking system will be in order, as well as a careful review of filtering possibilities of the higher-order derivatives of the heat-flux error. Finally, even though the *g-load* tracking was not required

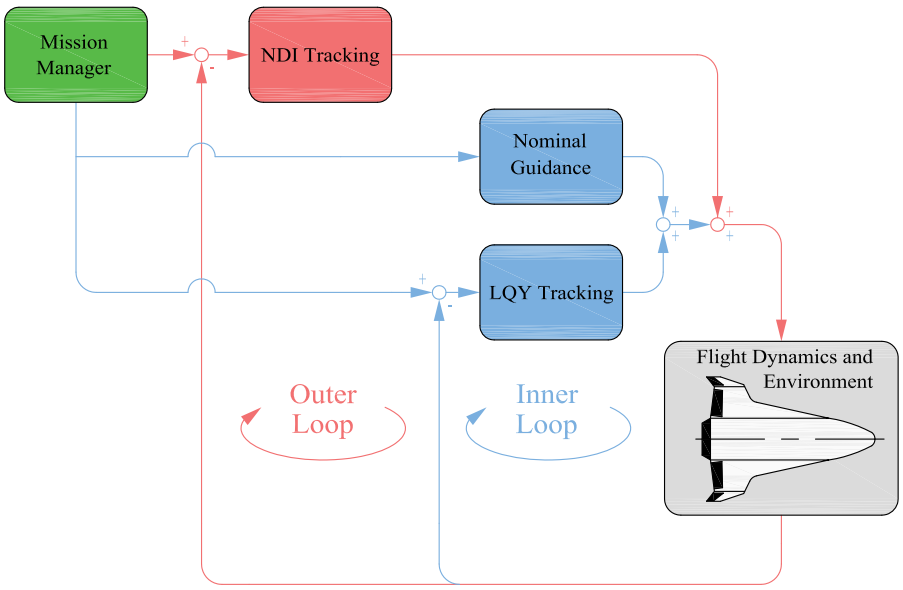

Figure 13. Integrated guidance system: nominal guidance plus LQY as inner loop, with outer-loop NDI tracking guidance.

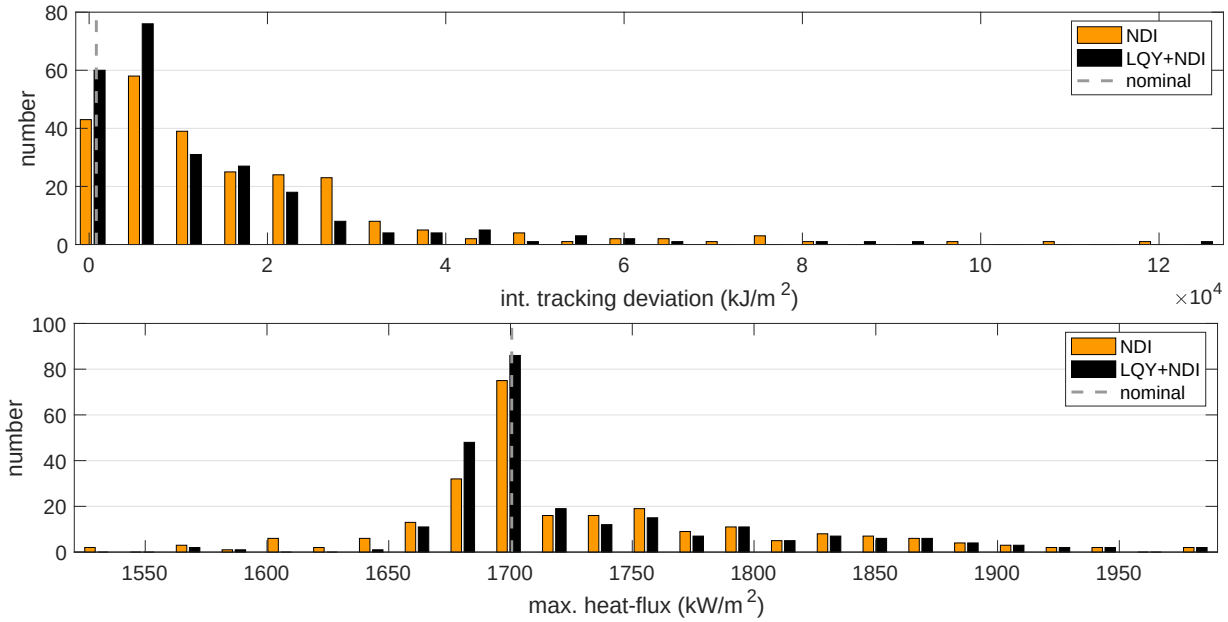

Figure 14. Integrated guidance: integrated tracking error and maximum heat flux (Monte-Carlo simulation with 250 runs).

right now, with a redesign of the nominal guidance this may no longer hold. Thus, along the same lines of the heat-flux tracking a similar design may be applied and then combined with the existing tracking system.

V. Conclusions and Outlook

In this paper the heat-flux tracking for a hypersonic test vehicle called *Hyperion-1*, is studied. Tracking is done by a non-linear dynamics inversion (NDI) controller applied to the error dynamics of the heat flux. Using the preliminary design, the tracking system is able to increase the tracking time by 200 s, which has

reduced the total integrated heat load by 30 MJ/m^2, albeit at the expense of some 200 km flight range, reducing it to 5827 km. During the preliminary analysis, a minor glitch in the nominal guidance was found to be responsible for exciting some small oscillatory behaviour in the commanded bank angle. This is related to the transition from heat-flux tracking to *g-load* tracking, that has to take place early in the flight due to the steep increase in *g-load* later on. A review of the already smooth transition is required. Also, extending the tracking at the end of the heat-flux plateau induces oscillations, since sudden changes in corrective bank angle are required. Removing this extension has solved that part of the oscillatory problem.

While doing a sensitivity analysis with variations in initial state, mass, aerodynamic coefficients and environmental properties, the tracking guidance performs robustly, and does better than the benchmark LQY (= linear quadratic regulator with output weighing) tracking system. Despite the large input variations, all output errors appear to be reasonable. A final design change, to combine the LQY tracking with the nominal guidance as inner loop, and the NDI tracking as outer loop improves the performance even more, making this a worthwhile guidance design to pursue further.

For near-future work, we have identified the following tasks. Reassessing the nominal guidance, and possibly a re-optimisation of the design parameters of the tracking system, as well as a careful review of filtering possibilities of the higher-order derivatives of the heat-flux error. Further, even though the *g-load* tracking was not required right now, with a redesign of the nominal guidance this may not be true any longer. Thus, in a similar fashion of the heat-flux tracking a comparable design may be applied and then integrated with the existing tracking system. Finally, the angle of attack has so far been used as an open-loop guidance command. It may serve a purpose to allow for a small corrective command to support the bank-angle tracking values. Since a change in angle of attack will directly affect both heat flux (and thus heat load) and the flight range, careful analysis of using the angle of attack like this is required.

References

[1]Schöttle, U.M. and Burkhardt, J., "Entwurf einer kleinen semiballistischen Rückkehrkapsel", Space Course, Lehrgang über Raumtransportsysteme, Stuttgart, 1995.

[2]Eggers, T., Longo, J., Hörschgen, M. and Stamminger, A., "The Hypersonic Flight Experiment SHEFEX", AIAA-2005-3294, *AIAA/CIRA 13th International Space Planes and Hypersonics Systems and Technologies Conference*, Capua, Italy, May 16-20, 2005.

[3]Börk, H., Dittert, C., Weihs, H., Thiele, T. and Guelhan, A., "Thermal Testing of the Sharp Leading Edge of SHEFEX II", AIAA-2012-5919, *18th AIAA/3AF International Space Planes and Hypersonic Systems and Technologies Conference*, Tours, France, 24-28 September, 2012.

[4]Börk, H., "Transpiration Cooling at Hypersonic Flight - AKTiV on SHEFEX II", AIAA-2014-2676, *11th AIAA/ASME Joint Thermophysics and Heat Transfer Conference*, Atlanta, GA, June 16-20, 2014.

[5]Sagliano, M., Samaany, M., Theil, S. and Mooij, E., "SHEFEX-3 Optimal Feedback Entry Guidance", AIAA Space2014 Conference, San Diego, CA, 4-7 August 2014.

[6]Mooij, E., Maree, A.G.M. and Sudmeijer, K.J., "Aerodynamic controllability of a selected re-entry test vehicle", IAF-95-V.4.04, *46^{t}h International Astronautical Congress*, Oslo, Norway, October 2-6, 1995.

[7]Mooij, E., "Adaptive Heat-Flux Tracking for Re-entry Guidance", AIAA-2014-4142, *AIAA/AAS Astrodynamics Specialist Conference*, San Diego, CA, August 4-7, 2014.

[8]Mooij, E., "Re-entry Guidance for Path-Constraint Tracking", AIAA-2017-1265, *AIAA SciTech 2017, Guidance, Navigation, and Control Conference*, Dallas, TX, January 6-10, 2017.

[9]Mooij, E., "Simple Adaptive Re-entry Guidance for Path-Constraint Tracking", AIAA-2018-1318, *AIAA SciTech 2018, Guidance, Navigation, and Control Conference*, Kissimmee, FL, January 8-12, 2018.

[10]Sieberling, S., Chu, Q.P., and Mulder, J.A., "Robust Flight Control Using Incremental Nonlinear Dynamic Inversion and Angular Acceleration Prediction", *Journal of Guidance, Control and Dynamics*, Vol. 33, No. 6, 2010, pp. 1732-1742.

[11]Acquatella, P., Falkena, W., Van Kampen, E.-J. and Chu, Q.P., "Robust Nonlinear Spacecraft Attitude Control using Incremental Nonlinear Dynamic Inversion", AIAA 2012-4623, *AIAA Guidance, Navigation, and Control Conference*, Minneapolis, Minnesota, 13-16 August 2012.

[12]Smeur, E.J.J., Chu, Q.P. and De Croon, G.C.H.E., "Adaptive Incremental Nonlinear Dynamic Inversion for Attitude Control of Micro Air Vehicles", *Journal of Guidance, Control, and Dynamics*, Vol. 39, No. 3, March 2016, pp. 450–460.

[13]Huang, Y., Pool, D.M., Stroosma, O. and Chu, Q.P., "Long-Stroke Hydraulic Robot Motion Control with Incremental Nonlinear Dynamic Inversion", *IEEE/ASME Transactions on Mechatronics*, Vol. 24, No. 1, February 2019, pp. 304–314.

Appendix A. State-Space Model

For constraint tracking, a (linearised) state-space model can be used, assuming that the deviation from the reference values (the *set points*) remain small. In short, we need to derive:

$$\Delta\dot{\mathbf{x}} = \mathbf{A}\Delta\mathbf{x} + \mathbf{B}\Delta\mathbf{u} \qquad \Delta\mathbf{y} = \mathbf{C}\Delta\mathbf{x} \tag{A1}$$

where the output is defined by q_c, Eq. (7), and n_g, Eq. (8). The $n \times n$ state or system matrix $\mathbf{A}$ and the $n \times m$ control or input matrix $\mathbf{B}$ follow directly from linearising the equations of motion. The states $\Delta\mathbf{x}$ representing translational motion are ΔV and Δh^*, which are the "controllable" states for vertical motion. As guidance parameters, $\Delta\mathbf{u}$, we only have the option to select the angle of attack, $\Delta\alpha$ and bank angle, $\Delta\sigma$, which are the two variables that define the magnitude and orientation of the aerodynamic force components (D and L)[a].

For the linearisation process the rotational rate of the Earth, ω_{cb} can be considered to be small and treated as a higher-order term. To save work, we will put $\omega_{cb} = 0$ before we start. The state equations to linearise are thus (see also Eqs. (1) and (6)):

$$\dot{V} = -g\sin\gamma - \frac{D}{m} \tag{A2}$$

$$\dot{h}^* = V\sin\gamma + c_\gamma\left(\frac{V^2}{R}\cos\gamma - g\cos\gamma + \frac{L}{m}\cos\sigma\right) + c_\gamma\gamma\dot{V} \tag{A3}$$

where we kept $\dot{V}$ in Eq. (A3) to facilitate the linearisation.

To formulate Eq. (A1), we begin with the state and input matrices, $\mathbf{A}$ and $\mathbf{B}$:

$$\mathbf{A} = \begin{bmatrix} \frac{\partial\dot{V}}{\partial V} & \frac{\partial\dot{V}}{\partial h^*} \\ \frac{\partial\dot{h}^*}{\partial V} & \frac{\partial\dot{h}^*}{\partial h^*} \end{bmatrix}_{\mathbf{x}=\mathbf{x_0},\mathbf{u}=\mathbf{u_0}} \quad \text{and} \quad \mathbf{B} = \begin{bmatrix} \frac{\partial\dot{V}}{\partial\alpha} & 0 \\ \frac{\partial\dot{h}^*}{\partial\alpha} & \frac{\partial\dot{h}^*}{\partial\sigma} \end{bmatrix}_{\mathbf{x}=\mathbf{x_0},\mathbf{u}=\mathbf{u_0}} \tag{A4}$$

which are evaluated at the nominal (typically trim) condition $\mathbf{x} = \mathbf{x_0}$ and $\mathbf{u} = \mathbf{u_0}$ (which will be indicated with $|_0$). Finally, to provide more insight in the outcome of the linearisation process the analytical exponential atmosphere is assumed. It is noted, though, that in case a more complex or even a tabulated density model is available, one could also use numerical differentiation to obtain the derivatives.

In earlier work,[7] the evaluation of the state derivatives shown in Eq. (A4) has been discussed in detail and will not be repeated here. However, for the sake of convenience the end result is given below.

$$\left.\frac{\partial\dot{V}}{\partial V}\right|_0 = g_0\frac{\gamma_0}{V_0}\cos\gamma_0 - \frac{1}{mV_0}\left\{M_0\frac{\partial C_D}{\partial M}\bar{q}_0 S_{ref} + D_0\left(2 - \frac{c_\gamma\gamma_0 V_0}{H_s}\right)\right\} \tag{A5}$$

$$\left.\frac{\partial\dot{V}}{\partial h^*}\right|_0 = -\frac{g_0}{c_\gamma V_0}\cos\gamma_0 + \frac{1}{H_s}\frac{D_0}{m} \tag{A6}$$

$$\begin{aligned}\left.\frac{\partial\dot{h}^*}{\partial V}\right|_0 =& \sin\gamma_0\left(1 - c_\gamma g_0\frac{\gamma_0}{V_0}\right) - \gamma_0\cos\gamma_0 + c_\gamma\gamma_0\frac{V_0}{R_0}\cos\gamma_0\left(\frac{2}{\gamma_0} + c_\gamma\frac{V_0}{R_0} + \tan\gamma_0\right) + \\ &+ c_\gamma\frac{\cos\sigma_0}{mV_0}\left\{M_0\frac{\partial C_L}{\partial M}\bar{q}_0 S_{ref} + L_0\left(2 - \frac{c_\gamma\gamma_0 V_0}{H_s}\right)\right\} + c_\gamma\gamma_0\left(\left.\frac{\partial\dot{V}}{\partial V}\right|_0 - \frac{\dot{V}_0}{V_0}\right)\end{aligned} \tag{A7}$$

$$\left.\frac{\partial\dot{h}^*}{\partial h^*}\right|_0 = \frac{\cos\gamma_0}{c_\gamma} - \frac{V_0}{R_0}\cos\gamma_0\left(c_\gamma\frac{V_0}{R_0} + \tan\gamma_0\right) + \frac{g_0}{V_0}\sin\gamma_0 + c_\gamma\frac{1}{H_s}\frac{L_0}{m}\cos\sigma_0 + \frac{\dot{V}_0}{V_0} + c_\gamma\gamma_0\left.\frac{\partial\dot{V}}{\partial h^*}\right|_0 \tag{A8}$$

The corresponding partials for $\Delta\alpha$ and $\Delta\sigma$ make up the control matrix $\mathbf{B}$:

[a] For the actual implementation one can decide to use both $\Delta\alpha$ and $\Delta\sigma$, where the contribution of each can be specified through weight selection, in combination with the dynamics relations. However, it may also be decided to use only a single guidance command; in that case the appropriate column of $\mathbf{B}$ shall be removed.

$$\mathbf{B} = \begin{bmatrix} -\frac{1}{m}\frac{\partial C_D}{\partial \alpha}\bar{q}_0 S_{ref} & 0 \\ c_\gamma \frac{\cos\sigma_0}{m}\frac{\partial C_L}{\partial \alpha}\bar{q}_0 S_{ref} & -c_\gamma \frac{L_0}{m}\sin\sigma_0 \end{bmatrix} \tag{A9}$$

Note that in case the nominal bank angle is zero, bank-angle tracking is not possible. Effectively, $\mathbf{B}$ changes then to a vector, retaining the first column of Eq. (A9). It is clear that the system is not fully controllable with just angle-of-attack control; while controlling one state one has to accept an error in the other one.

For the linearisation of q_c, Eq. (7) the density follows again an exponential profile. And, because the tracking guidance is only active when flying along the heat-flux constraint, $q_{c,setpoint}$, this value is of course the equilibrium value. The output matrix follows from linearising the output with respect to the states, *i.e.,*

$$\mathbf{C} = \left[\frac{\partial y}{\partial V} \quad \frac{\partial y}{\partial h^*}\right]_{\mathbf{x}=\mathbf{x_0},\mathbf{u}=\mathbf{u_0}} \tag{A10}$$

Consequently, linearising the output $\Delta y = \Delta q_c$ gives us for $\mathbf{C}$:

$$\mathbf{C} = q_{c,setpoint}\left[\frac{3}{V_0} - \frac{c_\gamma \gamma_0}{2H_s} \quad \frac{3}{c_\gamma \gamma_0 V_0} - \frac{1}{2H_s}\right] \tag{A11}$$

For output tracking, the *error* $\Delta\mathbf{y}$ should go to zero, which can be achieved by controlling the state, $\Delta\mathbf{x}$. Furthermore, once the setpoint has been reached, the error should remain zero, yielding that the error *derivative* should be zero as well. Since the output is not directly controllable, the idea is to bring Δy into a similar state-space form as Eq. (A1).

$$\Delta\mathbf{y} = \mathbf{C}\Delta\mathbf{x} \qquad \Rightarrow \qquad \Delta\dot{\mathbf{y}} = \dot{\mathbf{C}}\Delta\mathbf{x} + \mathbf{C}\Delta\dot{\mathbf{x}} \tag{A12}$$

with

$$\dot{\mathbf{C}} = q_{c,setpoint}\left[-3\frac{\dot{V}_0}{V_0^2} - \frac{c_\gamma}{2H_s}\dot{\gamma}_0 \quad -\frac{3}{c_\gamma}\left(\frac{\dot{\gamma}_0}{\gamma_0^2 V_0} + \frac{\dot{V}_0}{\gamma_0 V_0^2}\right)\right] \qquad \text{and} \qquad \Delta\dot{\mathbf{x}} = \mathbf{A}\Delta\mathbf{x} + \mathbf{B}\Delta\mathbf{u} \tag{A13}$$

Also, from Eqs. (1) and (2)

$$\dot{V}_0 = \omega_{cb}^2 R\sin\gamma_0 - g_0\sin\gamma_0 - \frac{D_0}{m} \tag{A14}$$

$$V_0\dot{\gamma}_0 = 2\omega_{cb}V_0 + \frac{V_0^2}{R_0}\cos\gamma_0 + \omega_{cb}^2 R_0\cos\gamma_0 - g_0\cos\gamma_0 + \frac{L_0}{m}\cos\sigma_0 \tag{A15}$$

$\Delta\dot{\mathbf{y}}$ is rewritten as:

$$\Delta\dot{\mathbf{y}} = \dot{\mathbf{C}}\Delta\mathbf{x} + \mathbf{C}\Delta\dot{\mathbf{x}} = \left(\dot{\mathbf{C}} + \mathbf{C}\mathbf{A}\right)\Delta\mathbf{x} + \mathbf{C}\mathbf{B}\Delta\mathbf{u} = \mathbf{A}^*\Delta\mathbf{x} + \mathbf{B}^*\Delta\mathbf{u} \tag{A16}$$

with

$$\mathbf{A}^* = \dot{\mathbf{C}} + \mathbf{C}\mathbf{A} \qquad \mathbf{B}^* = \mathbf{C}\mathbf{B} \tag{A17}$$

The second derivative of $\mathbf{y}$ would then follow from

$$\Delta\ddot{\mathbf{y}} = \ddot{\mathbf{C}}\Delta\mathbf{x} + 2\dot{\mathbf{C}}\Delta\dot{\mathbf{x}} + \mathbf{C}\Delta\ddot{\mathbf{x}} \tag{A18}$$

but to avoid having to write extensive formulas for this[b] we assume to have this parameter available through numerical differentiation.

[b]The expression for $\Delta\ddot{\mathbf{y}}$ includes the second derivative of $\Delta\mathbf{x}$ that can be obtained from the state-space formulation $\Delta\dot{\mathbf{x}} = \mathbf{A}\Delta\mathbf{x} + \mathbf{B}\Delta\mathbf{u}$:

$$\Delta\ddot{\mathbf{x}} = \dot{\mathbf{A}}\Delta\mathbf{x} + \mathbf{A}\Delta\dot{\mathbf{x}} + \dot{\mathbf{B}}\Delta\mathbf{u} + \mathbf{B}\Delta\dot{\mathbf{u}} \tag{A19}$$

or

$$\Delta\ddot{\mathbf{x}} = (\dot{\mathbf{A}} + \mathbf{A}^2)\Delta\mathbf{x} + (\mathbf{A}\mathbf{B} + \dot{\mathbf{B}})\Delta\mathbf{u} + \mathbf{B}\Delta\dot{\mathbf{u}} \tag{A20}$$

With an effort one can establish analytical expressions for most terms, apart from $\Delta\dot{\mathbf{u}}$, which has to be obtained numerically.